https://dx.doi.org/10.1016/j.commatsci.2022.111918

Atomistic investigation of modulating structural heterogeneities to achieve strength-ductility synergy in metallic glasses

Di Ouyang [a, b], Lei Zhao [a], Ning Li [b], Jie Pan [b], Lin Liu [b, *], K. C. Chan [a, *]

a Research Institute for Advanced Manufacturing, Department of Industrial and Systems Engineering, The Hong Kong Polytechnic University, Hung Hom, Kowloon, Hong Kong, 999077, China

b State Key Laboratory of Material Processing and Die & Mould Technology, School of Materials Science and Engineering, Huazhong University of Science and Technology, Wuhan, 430074, China

Abstract

Structural heterogeneities, i.e., spatial fluctuations of free volume, are of vital importance to the plasticity of irradiation-rejuvenated metallic glasses (MGs), but the mechanisms on how they affect the irreversible deformation and strength remain poorly understood. To address this issue, with the help of atomistic simulations, we systematically investigate the effect of structural heterogeneities on the mechanical behavior of tailored heterogenous MGs with uniformly distributed rejuvenated phases from several critical aspects such as pattern distribution, volume fraction and size effect. The results revealed that the periodically arranged soft rejuvenated phases with low diagonal orientation, high volume fraction and fine phase size alleviate the propensity of strain localization during the tensile deformation, hence promote the homogenous-like plastic flow mediated by the mass of homogenous shear transformation zones (STZ) operations. More importantly, the strength-ductility synergy of MGs was achieved at the given volume fraction of the rejuvenated phases via properly designing the arrangements of the heterogenous phases. The present study sheds light on the atomistic understanding of the relationship between the structural heterogeneity of rejuvenated amorphous structures and mechanical properties in MGs, which can provide useful insights for designing or processing

* Corresponding author: lliu2000@mail.hust.edu.cn (Lin Liu) and kc.chan@polyu.edu.hk (K.C. Chan)

MGs with a strength-ductility synergy.

***Keywords**:* Metallic glasses; Molecular dynamics; Structural heterogeneity; Mechanical properties

1. Introduction

Exhibiting intriguing mechanical and physical properties, such as high elasticity and strength and excellent wear and corrosion resistance, metallic glasses (MGs) offer exciting opportunities for various structural and functional applications benefiting from their disordered atomic arrangement [1-3]. Unfortunately, most MGs suffer from severe brittleness under tensile loading at ambient temperature. This is because, at lower temperatures ($<0.8T_g$, where T_g is the glass transition temperature), plastic deformation is usually inhomogeneous with plastic strain highly localized into some narrow regions (known as shear bands). Once initiated, shear bands become unstable and propagate rapidly, leading to limited macroscopic plasticity of the MGs before catastrophic fracture [4]. The severe brittleness of MGs restricts extensive applications as structural materials, and to eliminate this weakness, great efforts have been made to prepare ductile MGs. One effective method is to introduce structural heterogeneities, so that catastrophic propagation of shear bands at the early deformation stage is suppressed, more multiple shear bands are stimulated, and shear instability is postponed. Hence, greater plasticity is achieved before fracture in the MGs [5-7]. For instance, MG-matrix composites with outstanding plasticity were prepared by the ex-situ or in-situ introduction of ductile crystals, which act as obstacles to promote the formation of multiple shear bands and arrest the evolution of shear bands into micro-cracks [8, 9]. In addition, phase separation was verified to contribute in achieving a higher macroscopic plastic strain in MGs. This is because the localized shear bands are arrested within the nano-micro meter scale structural inhomogeneities in the amorphous matrix during deformation [10]. In addition, nanoglasses (NGs) with a network of glass-glass interfaces was observed to exhibit enhanced microscale tensile plasticity over the most rapidly melt quenched MG with the same chemical composition [11]. For a given MG,

structural inhomogeneities induced by surface pre-treatments were also proved to improve the plasticity of MG, such as laser surface treatment [12], shot peening [13], electrodeposition coating [14], and ultrasonic excitation [15]. In addition, rejuvenation treatment of MG is a converse process of aging to introduce structural inhomogeneities, which transforms the MG to their higher-energy states and significantly improves the deformation capability of MGs [16]. The rejuvenation methods include cryogenic thermal cycling [17], recovery annealing [18], high-pressure torsion [19] etc.

Besides the above-mentioned methods, ion bombardment has received extensive attention in recent years. This nondestructive treatment can enhance the spatially distributed structural heterogeneities of MGs at room temperature without changing the nature of the amorphous structure, so as to tailor the mechanical properties of MGs [20-22]. After ion bombardment (i.e., electron, protons or charged heavy ions), some regions in the amorphous phase of MGs can be rejuvenated to an extremely high energy state with increasing free volume content [23]. The equivalent cooling rate of irradiated metallic glass are 10^{13} K/s [24], significantly higher than that of the nanoglass (10^{9}~10^{10} K/s) [25]. Thus, the energy state of irradiation-induced rejuvenated phase is much larger than the nanoglass counterpart. Raghavan et al. [26] revealed that the deformation mechanism of the irradiated regions in Zr-based MG transformed from heterogeneous shear banding to homogeneous flow with the increasing Ni^{+} irradiation dosage due to the increasing severity of irradiation damage. Magagnosc et al. [27, 28] found that the initial brittle Pt-based MG nanowires can be tuned to a distinct glassy state upon Ga^{+} ion irradiation, leading to quasi-homogeneous plastic flow deformation and apparent tensile ductility. In addition, this behavior is reversible and the irradiated MG can return to the initial brittle state by annealing. Bian et al. [29] investigated the effect of irradiation dosage on the mechanical properties of Zr-based MG by using a Xe $^{26+}$ beam. They found that, at a low irradiation dosage, the irradiation-induced viscous flow results in the increasing of the free-volume fraction in the glassy phase, which decreases the hardness and yield strength of MG, as well as enhances its plastic deformation ability. While at a high irradiation dosage, the precipitation of the nano-particles easily builds up the stress concentration at the nanocrystal/glass interface and therefore reduces the tensile ductility. Chen et al. [30]

demonstrated that the strain rate sensitivity and plasticity of Zr-based MG can be tuned by He^+ ion irradiation. The enhanced strain rate sensitivity and plasticity are ascribed to the harmonious cooperation of larger-defects and small defects caused by ion irradiation. So far, although there have been few efforts devoted to understand the effect of ion irradiation on the mechanical properties of MGs, however, up to now, no study has systematically investigated the influence of the distribution of the irradiation-induced rejuvenated phases on the mechanical properties and deformation behavior of MGs. Since precisely tailoring the spatial distribution of rejuvenated phases is difficult, it is worthwhile to perform atomistic simulations to gain insights into the deformation mechanisms of MGs with tailored rejuvenated phases [5, 23, 31].

In our study, large-scale molecular dynamics (MD) simulations have been introduced to investigate the tensile deformation behavior of $Cu_{64}Zr_{36}$ (at.%) MGs with uniformly distributed irradiation-rejuvenated phases from several crucial aspects, such as pattern distribution, volume fraction and size effect. We demonstrate that the periodically arranged soft rejuvenated phases with low diagonal orientation, high volume fraction and fine phase size will alleviate the propensity of strain localization during the tensile deformation and restrain the formation of dominant shear band before sample yielding, so as to promote the homogenous-like plastic flow due to the mass of homogenous shear transformation zones (STZ) operations.

2. Simulation Methods

Classical MD simulations were implemented utilizing LAMMPS [32] combined with the validated CuZr potential developed by Cheng et al. [33]. A binary MG, $Cu_{64}Zr_{36}$ (at.%), was chosen due to its well-recorded atomic structure and deformation behaviour in the literature [34, 35]. A time step of 2 fs was used for all simulations. In addition, the Nosé-Hoover thermostat and barostat were adopted to control the temperature and pressure in the system under an isothermal-isobaric (NPT) ensemble [36]. In the first step, a small block of glass (30,000 atoms) was generated by quenching a fully homogenized $Cu_{64}Zr_{36}$ melt from 2000 K to the glass state (100 K) at a constant cooling rate of 10^{10} K/s under zero pressure and periodic boundary conditions (PBCs) in three dimensions. Next, the glass was replicated to obtain a large MG (50 × 4.8 × 100 nm^3 in the X-, Y- and Z-direction, respectively), which was further heated and

annealed at 800 K for 0.5 ns, and finally drawn back to 100 K. The obtained large glass sample (thereafter labelled as monolithic metallic glass (MMG)) contains 1.5 million atoms.

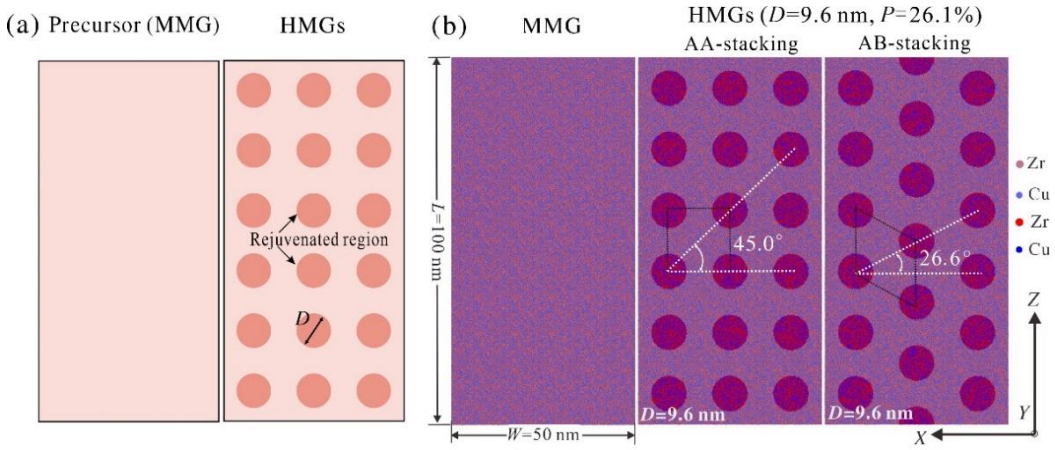

Fig. 1 (a) Schematics of the MMG and HMGs, illustrating the distribution of designed heterogenous structures; (b) Obtained atomic configurations of the MMG and two representative AA- and AB-stacked HMGs, the Cu and Zr type atoms in the multiplied regions were highlighted using darker colours compared to those in the matrix.

The hypothetical MGs imparted with various heterogeneous phases (thereafter referred as heterogeneous metallic glass (HMGs)) were prepared using the MMG as the precursor based on the schematics shown in **Fig. 1a**. Briefly, the imparted heterogenous phases were hypothesized to be columnar along the Z-direction (i.e., in round shape as observed from the XZ-plane), which were evenly distributed in the matrix. These soft heterogenous phases were still in full amorphous state but with a more rejuvenated structure than the precursor, which are regarded as the irradiation-induced rejuvenated phases with increasing free volume content and high energy state. To induce such heterogenous structure in the MG matrix, a "replaced-relax" procedure was executed on the atoms in the corresponding regions. To be more specific, 4.5% of Cu atoms and 8.0% of Zr atoms were assumed to be individually chosen in these regions, as reported in previous work [23]. These two groups of selected atoms were further set as the other type of atoms. Afterwards, the sample was isothermally relaxed at 100 K for a period up to 0.6 ns. It should be emphasized that the Zr and Cu atoms were swapped in the manipulated region in such a way that the composition remained unchanged, and the chemical heterogeneity

between the manipulated region and unmanipulated region was avoid. As uncovered in our previous study [23], such a manipulation of the local atomic configurations would introduce more excess free volume in the manipulated regions, inducing a rejuvenated structure because of the large disparity in atomic radius (1.60 Å vs. 1.28 Å) between the Zr and Cu atoms. Given that the size and number of the heterogenous phases in a glass is D and N, the total volume percentage of the heterogenous phases is then given by $P = \pi ND^2/(4WL)$, where W and L are the width and length of the glass, respectively. **Fig 1b** displays the atomic configurations of the MMG together with two representative HMGs, which have the same size (D = 9.6 nm) and volume percentage (P = 26.1%) of the rejuvenated heterogenous phases but with a difference in their pattern distributions, i.e., AA-stacking vs. AB-stacking. To achieve a comprehensive understanding of the intrinsic correlation between the structural heterogeneities and mechanical properties of MGs, we constructed a series of HMGs imparted with various combinations of sizes (D = 1.8 -14.4 nm), volume fractions (P = 0 - 58.63%) and pattern distributions (AA- vs. AB-stacking) of the rejuvenated phases through the same processing procedure.

Tensile simulations were further performed along the Z-direction at 100 K under a strain rate of 1×10^8 s^{-1} using an NPT ensemble. Before loading, the free surface condition was applied in the X-direction, while PBCs were set in the Y- and Z-direction. To characterize the atomic inelastic deformation, the atomic shear strain, η^{Mises} [37], was calculated and mointored utilizing OVITO [38]. It has been proven that η^{Mises} is a good micromechanical parameter to depict the local plastic deformation of MGs. Generally, regions with large η^{Mises} (i.e., $\eta^{Mise} > 0.3$) represent atom clusters undergoing inelastic rearrangements, and can be viewed as materials participating in STZs [39]. To achieve a quantitative interpretation of shear localization, the deformation participation ratio, $\psi = N^{\eta>0.3}/N$, and the degree of shear localization, $\phi = \sqrt{\sum_{i=1}^{N}(\eta_i - \eta_{ave})^2/N}$, are defined [23, 40, 41], where $N^{\eta>0.3}$ and N are the number of atoms participating in STZs and the total number of atoms in the sample, respectively; η_i represents the atomic shear strain of atom i, and η_{ave} is the averaged η^{Mises} over all atoms. For a glass experiencing uniform plastic deformation, ψ approaches 1 while ϕ approaches 0 [23].

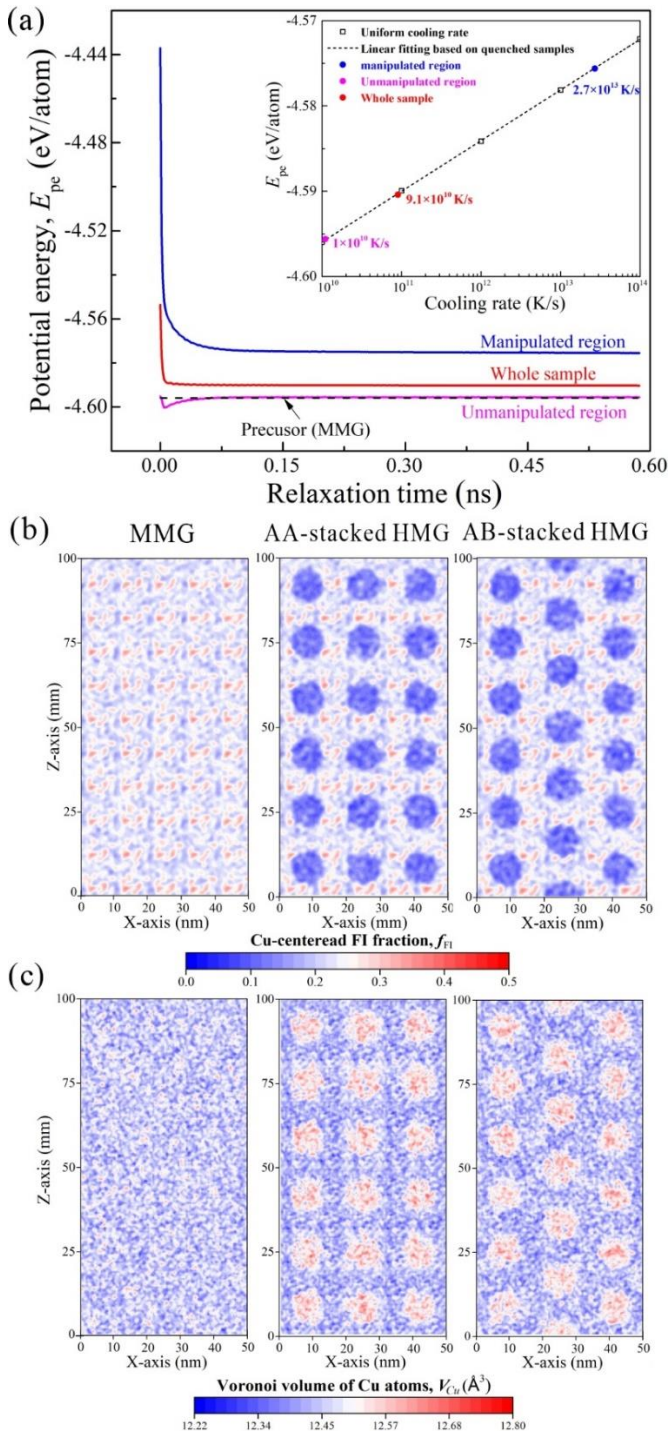

Fig. 2 Selected parameters revealing the structural features of the heterostructures in HMGs: (a) The evolutions of E_{pe} in the manipulated region, unmanipulated region and the whole sample for the AA-stacked HMG in the process of relaxation, the inset image shows E_{pe} as a function of the cooling rate for quenched glasses; The spatial heterogeneity revealed by the local variations of (b) f_{FI} and (c) V_{Cu} in the MMG (left-hand row), the AA-

(middle row) and AB-stacked HMGs (right-hand row) respectively, the bin sizes for sampling are 5.0 Å along the X- and Z-direction.

3. Results and discussion

3.1 Characterization of tailored structural heterogeneities in HMGs

The local structural modifications are expected to enhance the structural heterogeneities of MGs. As an illustration, the AA-stacked HMG shown in **Fig. 1b** is adopted to illustrate the structural state change after the modifications. The potential energy of a glass (E_{pe}) has been proven to strongly correlate with its processing history, and can be viewed as an effective parameter to describe the structural state [42]. The evolutions of the averaged E_{pe} of atoms in the manipulated region, unmanipulated region and the whole sample during the process of isothermal relaxation are shown in **Fig. 2a**. It can be seen that, E_{pe} as a function of the cooling rate for uniformly quenched glasses is displayed in the inset of **Fig. 2a**. One can see that all E_{pe} reach plateaus after relaxing for 0.5 ns, implying fully relaxed states of the constituted phases in the glass. After full relaxation, E_{pe} for the unmanipulated region (-4.5958 eV/atom) was still almost the same with the precursor, i.e., the MMG (-4.5960 eV/atom), while that for the manipulated region was significantly higher (-4.5756 eV/atom) due to the local structural modifications. Additionally, E_{pe} for the whole sample of the HMG is larger (-4.5904 eV/atom) than that of the MMG. These all suggest that the HMG was rejuvenated to a higher energy state, with the presence of two different states of glassy phases. The inset of **Fig. 2a** demonstrates that, for uniformly quenched glasses, E_{pe} exhibits an apparent logarithmic dependence on the cooling rate, which is well consistent with previous studies [42, 43]. To obtain the rejuvenated phases in the MMG, atomic manipulation was performed to achieve different energy states of amorphous phases by tuning the cooling rate. Similar methodology has been reported before, that assuming the linear relationship between the structural state of the phase and an equivalent cooling rate based on the measured E_{pe} [44]. As observed from the inset of **Fig. 2a**, the equivalent cooling rate for the manipulated region corresponds to a value of about 2.7×10^{13} K/s,

while that for the unmanipulated region is around 1.1×10^{10} K/s, which also corroborates a dual-phase heterostructure of the HMG.

To characterize the atomic structures of HMGs, the atomic topological structures are analyzed in terms of SROs utilizing Voronoi tessellation technology [45]. It has been demonstrated that Cu-centred full icosahedral (FI) clusters, i.e., Voronoi polyhedrons with index of <0,0,12,0> which yield a relatively high atomic packing density, are the prevailing structural motif of SROs in the Cu-rich $Cu_{64}Zr_{36}$ MG. They are responsible for the glass transition behaviour upon quenching and the strong-yet-brittle deformation behaviour upon mechanical loading [45, 46]. Therefore, the fraction of Cu-centred FI clusters within the Cu-type atoms (f_{FI}) is used as a parameter to describe the variation of the topological SROs behind the disordered structures. In addition, the relative change of the Voronoi volume of Cu-type atoms (V_{Cu}) is adopted to assess the free volume distribution, since the former is expected to scale with the latter [47, 48]. **Fig. 2b-c** displays the spatial distributions of f_{FI} and V_{Cu} in the representative AA- and AB-stacked HMG presented in **Fig. 1b**, together the as-quenched MMG for comparison. The MMG demonstrates some spatial fluctuations of f_{FI} and V_{Cu} values beyond the atomic scale. These fluctuations indicate the presence of intrinsic structural heterogeneities in the as-quenched MG. Such structural heterogeneities at a length scale of several nanometers have been reported in previous atomistic simulations [49, 50] and also verified experimentally by probing the nanoscale fluctuations in local elastic and viscoelastic (i.e., damping) properties using advanced atomic force microscopy technologies [51-53]. After the local structural modifications, it can be seen that the nanoscale fluctuations are greatly enhanced. The manipulated regions in the two HMGs are depicted by a relatively lower f_{FI} and a relatively higher V_{Cu} in comparison with the surrounding matrix and the MMG. More specifically, the average f_{FI} and V_{Cu} in the surrounding matrix are 24.2% and 12.45 $Å^3$, while those in the manipulated regions are 12.8% and 12.51 $Å^3$, respectively. It is clear that local atomic rearrangements in the manipulated regions destroy the Cu-centered FI clusters and induce more access free volume, similar to that occurring in the process of collision cascades during ion irradiation [23]. The HMGs exhibit a characteristic of tailored heterogenous structures with a higher degree of structural rejuvenation, which points to a more liquid-like and softer state. The

imparted rejuvenated phases characterised with a higher equivalent cooling rate promote the structural heterogeneities behind the amorphous structures and can lead to a significant change of the mechanical properties under loading [23, 54]. In the following sections, we aim to investigate the effect of structural heterogeneities, in the form of various combinations of pattern distribution, volume fraction and size effect of the rejuvenated phases, on the mechanical properties of HMGs.

3.2 Effect of AA- vs. AB-stacked distribution of rejuvenated phases

The first question we address is whether the arrangements of the rejuvenated phases affect the strength and ductility of HMGs. The AA- and AB-stacked HMGs shown in **Fig. 1b** were chosen for analysis. Note that these two HMGs were constructed with the same size (D = 9.6 nm) and volume fraction (P = 26.1%) of heterogenous phases but differing in their arrangements. The phase size was chosen to be comparable to the SB width (~10 nm), which was expected to promote the interactions between SBs and heterogenous phases [55, 56]. As shown in **Fig. 1b**, the different arrangements result in an angle of 45.0° and 26.6° between the diagonal direction of heterogenous phases and the X-direction for the AA- and AB-stacked HMGs, respectively.

Fig. 3a depicts the tensile strain-stress curves for the two HMGs. In accordance with previous studies [5, 23], the peak stress (σ_p) is regarded as the threshold stress for triggering macroscopic plastic flow at the macroscopic yield point (ε_p), i.e., corresponding to the macroscopic yield strength. It can be observed that the stress-strain curves nearly overlap before ε_p = 6.8% (i.e., at the elastic deformation stage) but gradually deviat from each other after ε_p (i.e., at the plastic deformation stage). The macroscopic yield points (ε_p) and yield strengths (σ_p) are almost identical. Nevertheless, the AB-stacked HMG exhibits a higher flow stress and slower stress drop at the plastic deformation stage, a manifestation of a tendency toward shear delocalization [23, 57]. To achieve a quantitative understanding of the plastic behavior, **Fig. 3b** presents the evolutions of ψ and ϕ (see **Simulation Methods**) as a function of the applied strain (ε). Generally, a larger value in ψ indicate that a higher fraction of atoms participate in plastic deformation in a glass, and a larger value in ϕ suggests a higher propensity of strain localization

through individual SBs. It is seen that, although ψ and ϕ are nearly the same for both HMGs before ε < 9%, a higher ψ combined with a smaller ϕ at the post-yielding stage (ε >9%) can be observed for the AB-stacked HMG. This remainds us of the better tensile ductility for the AB-stacked HMG as revealed in the stress-strain curves shown in **Fig. 3a**. We have also examined several other AA- and AB-stacked HMGs, which have different sizes (i.e., different volume fractions) of heterogenous phases. The results (not shown here) are analogous to the illustration presented above. It can be concluded that the arrangements of the rejuvenated phases barely affect the elastic behavior but have a nonnegligible effect on the plastic behavior of HMGs, more specifically, the AB-stacked one is more effective at promoting strain delocalization.

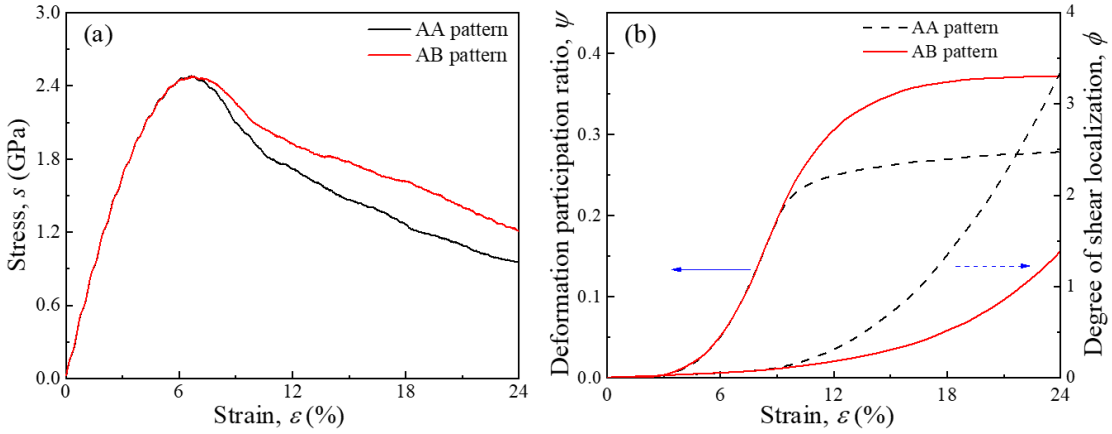

Fig. 3 (a) The tensile stress-strain curves of the AA- and AB-patterned HMGs; (b) The evolution of ψ (left Y-axis) and ϕ (right Y-axis) as a function of the applied strain.

To elucidate the underlying deformation mechanisms, **Fig. 4a-c** demonstrates a sequence of deformation snapshots for the AA- and AB-stacked HMGs, colored by η^{Mises}. For clarity, only atoms with η^{Mises}> 0.3 are displayed. In addition, the geometric profiles of the rejuvenated phases were rendered and monitored using the surface mesh technology, as implemented in Ovito [38]. It can be easily observed that, although both HMGs fail via one dominant SB, the AB-stacked one displays a higher number of secondary SBs and a smaller shear offset at the end of the deformation (see ε = 24% in **Fig. 4a-c**). It is meaningful to analyze the similarities and differences behind their deformation behavior. For both samples, STZs are first triggered in the rejuvenated phases and on the lateral surfaces due to their relatively higher energy state

and softer structures, which will act as the nucleation regions of SBs [58] (see ε = 5.2% in **Fig. 4a-c**). As the deformation proceeds, these STZs are inclined to dispersedly proliferate to higher density without quick aggregation. It is not until the applied strain approaches to the macroscopic yield point (i.e., ε = 6.8%) that STZs begin to be activated in the surrounding matrix. It is worth noting that these STZs tend to emerge regularly between the diagonal regions of the periodically arranged heterogenous phases for both samples (see ε = 7.0% in **Fig. 4a-c**). These STZs aggregate and grow progressively upon further loading. When some of the STZs reach a critical size that is comparable to the SB width, SB nucleation occurs. The formed embryonic SBs in the hard matrix tend to propagate bilaterally to the neighboring rejuvenated phases and further impede these phases soon after formation (see ε = 7.8% and 9.0% in **Fig. 4a-c**). It should be mentioned that in such circumstances the rejuvenated phases can retard the shear banding dynamics via the mechanism of altering the autocatalytic percolation of STZs in the shear front due to the structural differences and elastic fluctuations between the soft and hard phases, as recently revealed by Şopu et al. [59]. The suppression of rapid formation of a critical SB by the rejuvenated phases, in turn, promotes more embryonic SBs, participating in plastic deformation (see ε = 9.0% and 15.0% in **Fig. 4a-c**). However, due to the small total volume fraction of the rejuvenated phases (26.1%), for both HMGs, one dominant SB is still formed at the end, which penetrates all rejuvenated phases along one diagonal direction of the phases (see the deformed atomic configurations marked in **Fig. 4b-d**) and induces apparent shear offsets.

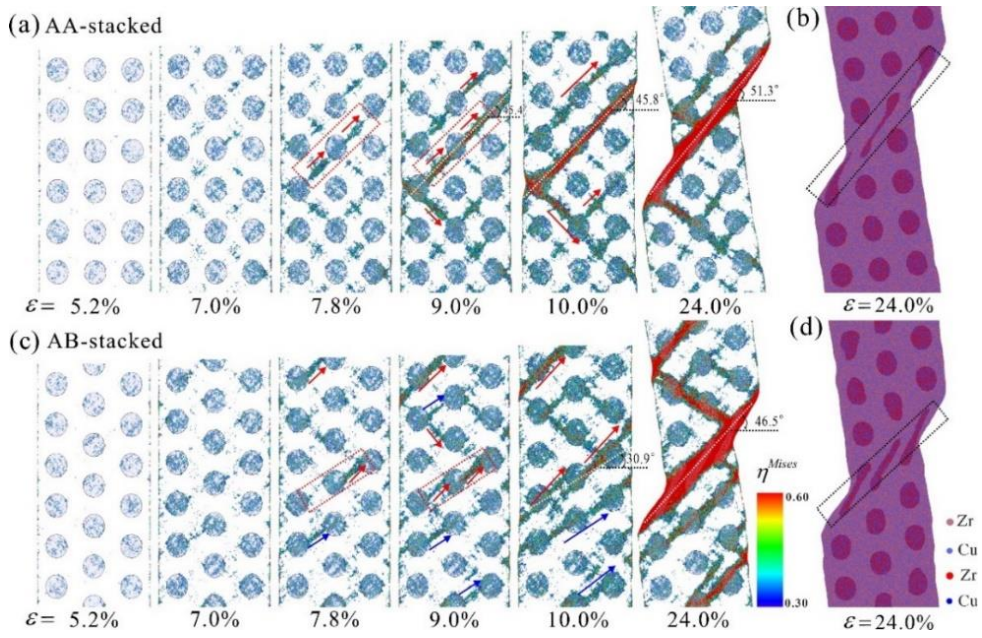

Fig. 4 Illustrations of the plastic deformation processes for AA- and AB-stacked HMGs, which have the same volume fraction (26.1%) and size (9.6 nm) of heterogeneous phases: (a) and (c) Representative snapshots of η^{Mises} at different applied strain showing the deformation and failure of the two HMGs. For clarity, only atoms with η^{Mises}> 0.3 are displayed. The colors indicate the atomic shear strain within the defined range of values. The red arrows denote SBs orientated along the principal shear stress direction, while the blue arrows mark SBs orientated along the angle of 26.6°; (b) and (d) represent the atomic configurations of the two HMGs at the end of loading.

Behind these similarities, one can also notice some distinct differences in the detailed shear processes of the AA- and AB-stacked HMGs, owing to the different diagonal orientations (45.0° vs. 26.6°) of the periodically arranged heterogenous phases. It is well established that SBs tend to propagate along a shear path approximately following the principal shear stress plane in MGs [23, 60]. For the AA-stacked HMG, the rejuvenated phases are just arranged diagonally periodic along the principal shear stress plane. Therefore, upon loading, embryonic SBs between the soft phases can easily align and connect with each other, forming a critical SB along the principal shear stress plane (see the marked regions at ε=7.8% and 9.0% in **Fig. 4a**).

Despite these soft phases located on the shear path impeding the rapid propagation of the critical SB, only a few extra SBs are triggered before the failure of the sample via the critical SB (see at ε=24% in **Fig. 4a**). Moreover, due to the strong relative motion between the upper and lower parts of the sample, the angle of the critical SB with respect to the X-direction, i.e., the fracture angle, reaches a value as large as 51.3° at ε = 24%. In contrast, the diagonal orientation of the periodically arranged soft phases is reduced to 26.6° for the AB-stacked HMG. The large angle deviation results in competition for SBs to propagate along two characteristic directions, i.e., along the principal shear stress direction (45°) and along the diagonal direction of the heterogenous phases (26.6°), similar to that observed in MG heterostructures with AB-stacked nanopores [61]. One can clearly see the co-existence of these two types of embryonic SBs in the AB-stacked HMG at ε > 7.8% (see the representative embryonic SBs marked in red and blue arrows in **Fig. 4c**). Notably, the competition results in the formation of the critical SB that deviates from the principal shear stress direction, leading to the formation of multiple SBs and a lower energy state in the critical SB. Meanwhile, the SB width is also much larger than that observed in the AA-stacked counterpart, since the critical SB is formed by the coalescence of unaligned embryonic SBs between adjacent rejuvenated phases almost along the diagonal direction (30.9° at ε = 10%). The large deviation angle from the principal shear stress and the thickening of the critical SB reduces the elastic energy release for unstable shear localization, promoting the propagation of more SBs (see ε = 24.0% in **Fig. 4c**). Since multiple SBs are involved in plasticity in the AB-stacked HMG, the resultant shear offset and fracture angle (46.5° vs. 51.3°) are smaller than those observed in the AA-stacked counterpart. This process of shear delocalization reliefs strain-induced softening [23, 55], thereby alleviating the magnitude of stress drop for the AB-stacked HMG, which can be corroborated from its stress-strain curve shown in **Fig. 3a**. From the above analysis, it is clear that the tensile ductility of HMGs can be effectively improved without the sacrifice of strength at the given volume fraction of the heterogenous phases via properly designing the arrangements of heterogenous phases. In the previous literature, several works associated with the design and optimization of MG composites also reported that the plastic deformability of MGs tailored with various other

forms of heterogenous phases (e.g., crystalline metals [62, 63], nanoglass [64] and pore [61, 65]) can be improved using the AB-stacking strategy.

3.3 Effect of the volume fraction of rejuvenated phases

It has been reported that introducing soft heterogenous phases, such as Cu crystals, in MGs are capable of enhancing the plasticity but inevitably at the sacrifice of the strength of MGs [62]. The introduction of rejuvenated amorphous phases in the precursor is also anticipated to detract its strength. Therefore, the next question we address is to what extent the volume fraction of the rejuvenated phases affects the strength and tensile ductility of MGs. To this end, we fabricated ten HMGs, which have the same rearrangement of the rejuvenated phases (N =18 and AB-stacking) but with the phase size spanning from 3.6 nm to 14.4 nm, at intervals of 1.2 nm. The corresponding volume fraction of the rejuvenated phases in this series of HMGs ranges from 3.7% to 58.6%.

Fig. 5a depicts the tensile stress-strain curves for the series of AB-stacked HMGs, along with the MMG for comparison. The inset of **Fig. 5a** shows several representatives of these HMGs with different volume fractions of the rejuvenated phases. Several distinct features can be seen from **Fig. 5a**. Firstly, ε_p for the MMG and HMGs are almost identical (6.8%), suggesting that the critical macroscopic yield point is independent of the volume fraction of the rejuvenated phases. This is quite unlike the cases for MG composites with other forms of heterogenous phases, such as Cu crystals [62, 63], in which a decrease of ε_p with increasing volume fraction of these heterogenous phases are usually observed. This discrepancy is ascribed to the large differences in elastic modules and critical yield points between these heterogenous phases and the MG matrix, which promote earlier yielding of the MG matrix [62]. The second feature is that σ_p decreases progressively with the increasing volume fraction of the rejuvenated phases. This indicates a softening tendency of the glasses after introducing the rejuvenated phases. The variation of σ_p as a function of volume fraction of the rejuvenated phases, presented in **Fig. 5b**, further reveals a linear relationship in the series of HMGs. The third feature is that the amplitude of the stress drop upon yielding decreases gradually, while the flow stress at the post-yielding stage increases inversely with increasing volume fraction from 0% to 58.6%. For the MMG,

the stress-strain curve clearly displays a drastic stress drop after the macroscopic yielding, which is associated with the rapid localization of plastic strain into one dominant SB [23]. The large stress drop and low flow stress are generally viewed as the features of the poor plasticity of MGs [5, 54]. While, for the HMGs with volume fraction exceeds 33.0%, the stress drop is almost weak and the flow stress maintains a relatively steady value at large ε, which indicate an obvious change in the deformation mode [23, 62].

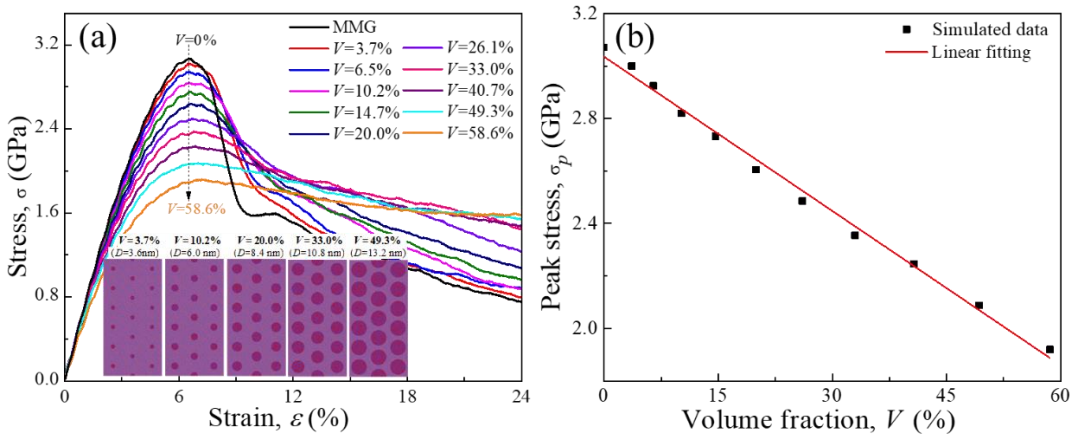

Fig. 5 (a) Tensile strain-stress curves for the AB-patterned HMGs tailored with different volume fractions of heterogeneous phases, the inset images show the atomic configurations of several representative HMGs; (b) The variation of σ_p as a function of the volume fraction of heterogeneous phases.

The contrast in deformation behavior with different volume fractions of the heterogeneous phases can be also observed in **Fig. 6**, in which the evolutions of ψ as a function of the applied strain for the series of HMGs are presented. One can see that, for the MMG, ψ reaches a low plateau soon after yielding and maintains the value for the rest of the plastic deformation. This is because the plasticity of the MMG is confined in one dominant SB soon after its formation. By increasing the volume fraction of the rejuvenated phases from 3.7% to 58.6% in the HMGs, ψ is augmented in a manner more proportional to the applied strain, implying that more materials are involved in plasticity. The variation of ϕ with respect to the volume fraction of the rejuvenated phases at the end of deformation, displayed in the inset of **Fig. 6**, demonstrates that ϕ is gradually reduced with increasing the volume fraction, which suggests a tendency of

delocalized plastic deformation of these HMGs. Moreover, when the volume fraction reaches 49.3%, ϕ decreases to a value that approaches 0, a manifestation of homogenous-like plastic flow behaviour [23]. These results all imply the presence of a brittle-to-ductile transition of the deformation mode in HMGs with increasing volume fraction of rejuvenated phases from 0% to 58.6%.

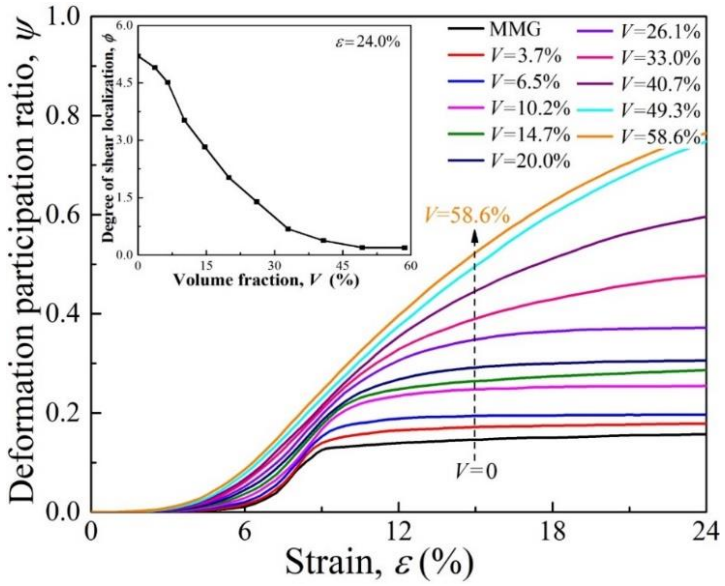

Fig. 6 The evolution of ψ as a function of applied strain in the AB-stacked HMGs with different volume fractions of heterogeneous phases, the inset image shows the degree of shear localization ϕ vs. the volume fraction at ε = 24.0%.

It is accepted that the occurrence of strain delocalization in MG is associated with the competition between the macroscopic yield strength (σ_p) of the material and the critical stress (σ_c) required for activating the aggregation of STZs and forming a mature shear band [5, 66]. If σ_c cannot be attained under successive deformation, the propagation of the embryonic shear bands would be immediately restrained upon their formation [23]. In the present HMG, σ_c is an intrinsic parameter around 2.34 GPa [23], σ_p is gradually decreased with the enhanced volume fraction of rejuvenated phases. For the HMGs with volume fraction from 0% to 26.1%, $\sigma_p > \sigma_c$, the resultant σ_p is sufficient to overcome the intrinsic resistance to the formation of mature shear bands. Thus, the deformation patterns of these HMGs are featured by the individual highly localized shear process. While for the HMGs with volume fraction higher than 33.0%, $\sigma_p < \sigma_c$,

highly localized shear banding tends to be restrained, and homogeneous-like plastic flow is achieved. To understand the above-mentioned transition, **Fig. 7** presents the deformation snapshots for the MMG (the 1st column) and three AB-stacked HMGs (the 2nd - 4th columns) with various rejuvenated phase sizes of 6.0 nm, 10.8 nm and 13.2 nm, which correspond to a series of volume fractions of 10.2%, 33.0% and 49.3%, respectively. One can see that the moment when critical SBs forms gradually delay, and fully disappear when the volume fraction reaches 49.3%. As expected, there exists a transition of the deformation mode from highly localized shear banding to homogeneous-like plastic flow. For the MMG, one embryonic SB forms on the free surface soon after the macroscopic yielding. The embryonic SB propagates along the principal shear stress plane without any resistance and penetrates into the sample over a small strain increment, which is consistent with previous studies [45, 60]. For the HMG with a relatively low volume fraction of 10.2%, multiple embryonic SBs are induced between the rejuvenated phases after macroscopic yielding (see ε = 9.0% in the 2nd column). However, due to the relatively smaller size (D = 6.0 nm) relative to the SB width, the rejuvenated phases cannot block the propagation of the embryonic SBs upon further loading. Instead, one mature SB forms at large ε by connecting the embryonic SBs (marked by the box at ε = 9.0%) along the diagonal orientation, absorbing the rejuvenated phases in the shear path (see ε = 12.0% in the 2nd column). As a result, the plastic deformation of this HMG is dominated by one mature SB and a large shear offset is induced. Similar to the size effect of crystalline precipitates observed in MG composites [67, 68], the effect of rejuvenated phases on SB propagation in HMGs is expected to be strengthened with increasing phase size (i.e., the volume fraction in this case). When the volume fraction increases to 33.0%, the rejuvenated phases (D = 10.8 nm) are sufficiently large to serve as effective barriers to suppress SB propagation across the rejuvenated phases. It is noted that hindering the propagation of earlier-formed SBs by the rejuvenated phases would promote the activation of new SBs, which may propagate along different directions. This leads to the formation of a network of multiple SBs without one becoming critical (see ε = 24.0% in the 2nd column). The formation and interaction of multiple SBs could considerably stabilize the plastic deformation process [69], which thus greatly alleviates the rate of stress drop in the stress-strain curve in the HMG, as evidenced in **Fig. 5a**.

When the volume fraction reaches a value as high as 49.3%, it is noted that the distance between two neighboring rejuvenated phases is only ~ 5.4 nm, which is much lower than the SB width. In such circumstances, the limited volume of materials between the neighboring rejuvenated phases constrain the initiation of local embryonic SBs (see ε = 12.0% in the 4th column). As demonstrated above, the formation of mature SBs carrying the plasticity in the HMGs heavily relies on the initiation of embryonic SBs in the MG matrix. Since no shear banding event occurs in the MG matrix, the HMG exhibits a homogenous-like plastic flow mediated by homogenous STZ operations, both in the MG matrix and rejuvenated phases at large ε. One can see that the direct observation of the transition of the deformation mode from the deformation snapshots of these HMGs is very consistent with the contrasting stress-strain curves shown in **Fig. 5a**.

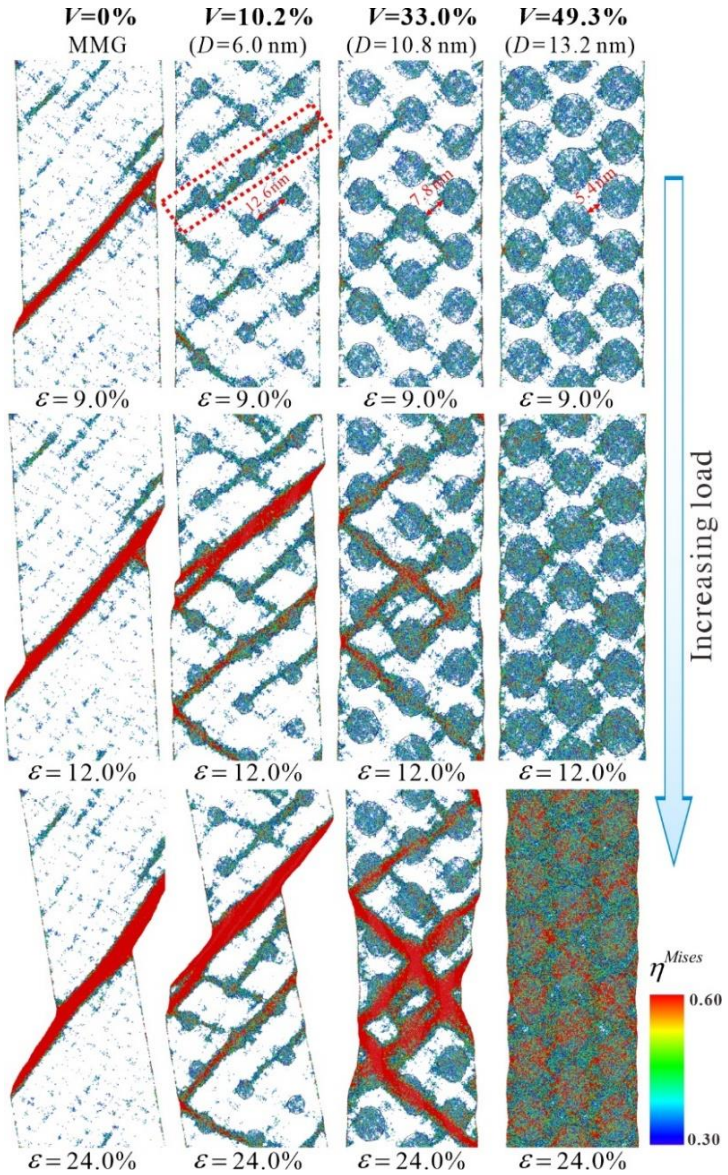

Fig. 7 The deformation patterns of the MMG (the first column) and several representative AB-stacked HMGs (from the second to the fourth columns) under different applied strains, illustrating a transition of the deformation mode with increasing volume fraction of the rejuvenated phases.

3.4 Effect of the phase size of rejuvenated phases

In the above simulations, a small number (N = 18) of rejuvenated phases is adapted to better illustrate the effect of the rejuvenated phases on the shear banding process in HMGs. However, it is unclear whether the number of rejuvenated phases can also influence the mechanical properties of HMGs or not. It should be noted that increasing the number of rejuvenated phases is expected to reduce the phase size, leading to a more dispersed distribution of the rejuvenated phases throughout the samples. To examine the phase size effect, we constructed a series of AB-stacked HMGs, which have the same volume fraction of the rejuvenated phases (26.1%) but with the phase numbers ranging from 8 to 512. The phase size (D) and number (N) obeys the relationship $D^2 \propto 1/N$ .The phase size in this series of HMGs spans from 14.4 nm (N = 8) to 1.8 nm (N = 512).

Fig. 8a displays the stress-strain curves for the series of AB-stacked HMGs with the same volume fraction of 26.1%. The inset of **Fig. 8a** presents the atomic configurations of several representative HMGs. In addition, **Fig. 8b** plots the evolution of σ_p as a function of the number of rejuvenated phases, together with the stress-strain response near the peak, demonstrated in its inset. It is seen that, with increasing the number of rejuvenated phases in the HMGs (i.e., decreasing the phase size in this case), σ_p maintains the same value of 2.48 GPa when $N \leq 128$ and then reduces slightly to a value of 2.40 GPa when N increases to 512. The small variation of σ_p over a large range of N implies that the macroscopic yield strength of HMGs is almost independent of the phase size at the given volume fraction of the rejuvenated phase. However, an intriguing observation from **Fig. 8a** is that the rate of the stress drop at the post-yielding stage in these HMGs decreases progressively, an indication of a tendency for shear delocalization [23]. The evolution of σ_p and the rate of the stress drop clearly suggest that the

tensile ductility of HMGs can be improved by decreasing the phase size of the rejuvenated phases without sacrifice of the strength.

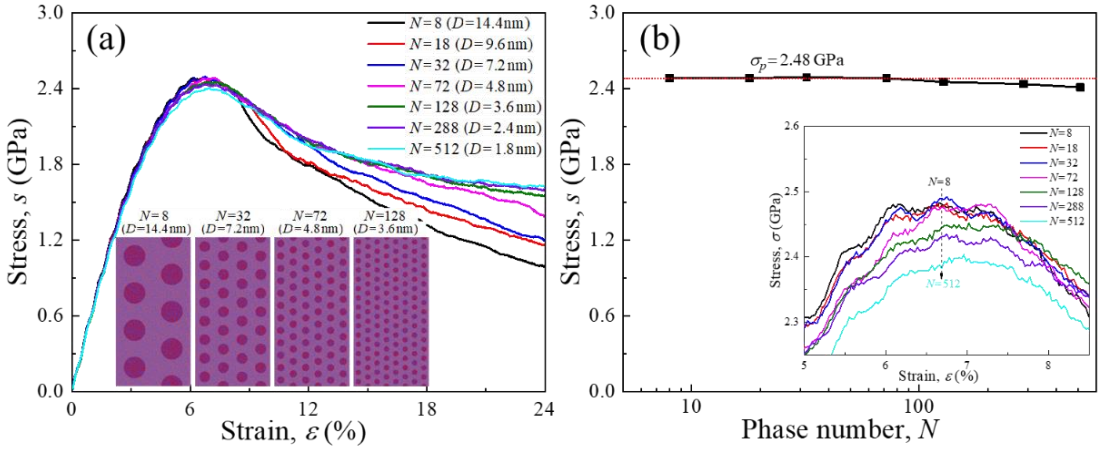

Fig. 8 (a) Tensile strain-stress curves for the AB-patterned HMGs with various heterogeneous phases having the same volume fraction of (26.1%) but different phase sizes (1.8 - 14.4 nm), the inset images show the atomic configurations of several representative HMGs; (b) The variation of σ_p as a function of the volume fraction of heterogeneous phases, the inset image shows the strain-stress curves near the peak stress.

To better understand the shear delocalization process in the series of HMGs, **Fig. 9** presents the evolution of ψ as a function of the applied strain. In addition, the inset of **Fig. 9** demostrates the change of ϕ at ε = 24.0% as a function of the phase number. The ψ value are almost the same for the series of HMGs at any applied strain during the elastic deformation stage and at the early plastic deformation stage (i.e., at ε < 10%). This is significantly different from the case for the HMGs with different volume fractions of the rejuvenated phases shown in **Fig. 6**. The same ψ at ε < 10% indicates that the amount of activated STZs, which contributes to the initial plasticity of HMGs, is barely influenced by the phase size at the given volume fraction of the rejuvenated phases. Hence, one can observe the same macroscopic yield strength for these HMGs in the stress-strain curves shown in **Fig. 8a**. However, when ε > 10%, the variations of ψ begin to deviate from each other. For the HMGs with a finer phase size of the rejuvenated phases, ψ is larger at any given applied strain, indicating a higher proportion of

materials involved in plastic deformation. Correspondingly, the change of ϕ at ε = 24.0%, shown in the inset of **Fig. 9**, reveals a decreasing trend of ϕ with the phase number, unambiguously signifying a process of strain delocalization. The evolutions of ψ and ϕ further confirm a tendency of improved tensile ductility with increasing phase number in these HMGs with the same volume fraction of the rejuvenated phases.

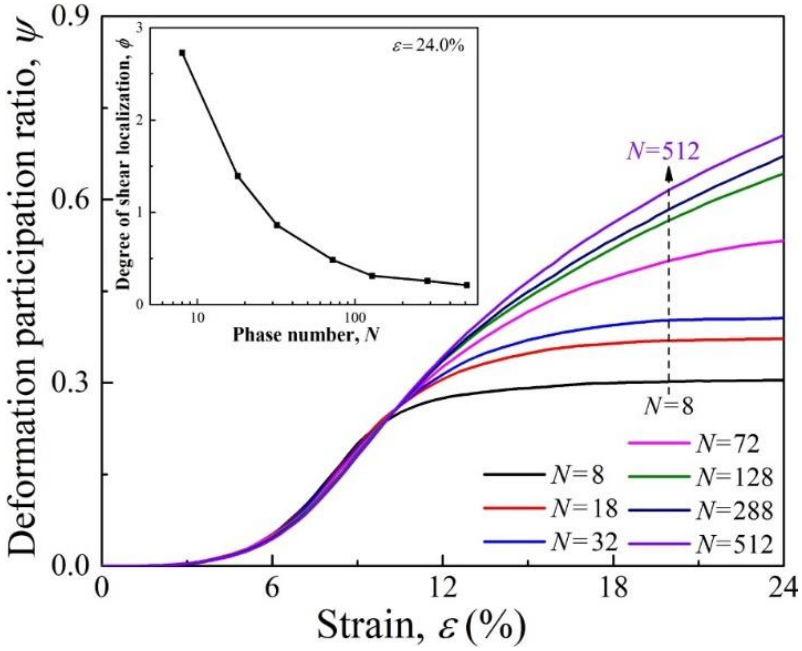

Fig. 9 The evolution of η (left Y-axis) and ϕ (right Y-axis) for the AB-patterned HMGs with various heterogeneous phases having the same volume fraction of (26.1%) but different phase sizes (1.8 - 14.4 nm).

To understand the above-mentioned ductility enhancement, **Fig. 10** presents the deformation snapshots of the four representative HMGs shown in the inset of **Fig. 8a**, which have different phase numbers of 8 (D =14.4 nm), 32 (D = 7.2 nm), 72 (D =4.8 nm) and 128 (D = 3.6 nm), respectively. One can clearly observe a transition of the deformation mode from highly localized shear banding to homogeneous-like plastic flow in these HMGs. At the early deformation stage, STZs are first initiated in the rejuvenated phases and further in the MG matrix between the rejuvenated phases, following the same deformation process of the AB-stacked HMGs, as shown in **Fig. 4** and **Fig. 7**. With increasing phase number, the rejuvenated phases are distributed more homogenously in HMGs. This leads to the formation of more

dispersive STZs throughout the sample at the same applied strain (see ε = 9.0% in **Fig. 10**), despite the amounts of activated STZs being nearly identical for all the HMGs before ε = 10.0%. It is noted that more dispersed STZs at the early deformation stage promote the activation of embryonic SBs and new STZs with further deformation (see the second row in **Fig. 10**), which could redistribute more plasticity throughout the sample [5]. For the HMGs with low phase numbers of 8 and 32, only a few SBs are generated at the post-yielding stage (see ε = 12.0%), despite having they have relative large sizes of the rejuvenated phases. The failure of these two glasses is still governed by plastic shearing of one dominant SB, a signature of substantial brittleness also observed in the HMG. While for the HMG with a relatively large phase number of 72, a high density of embryonic SBs together with fertile STZs are induced at the post-yielding stage (see ε = 14.4%). As the deformation proceeds, these embryonic SBs deform and interact with each other cooperatively, leading to a tendency of necking behavior at the end of deformation. When further enlarging the phase number to a value as large as 128, it appears that STZs cannot effectively localize into embryonic SBs in the HMG due to the highly dispersed distribution of the rejuvenated phase. In this case, the continuous activation of new STZs throughout the sample is favored over the formation of embryonic SBs. Therefore, a homogenous-like plastic flow mediated by homogenous STZ operations is observed for this HMG. To sum up, the microstructure design strategy of MGes is that the stacked patterns with low diagonal orientation, larger volume fraction of rejuvenated phase and finer rejuvenated phase size are benefit to promote strain delocalization, so as to improve the plasticity and ductility of MGs.

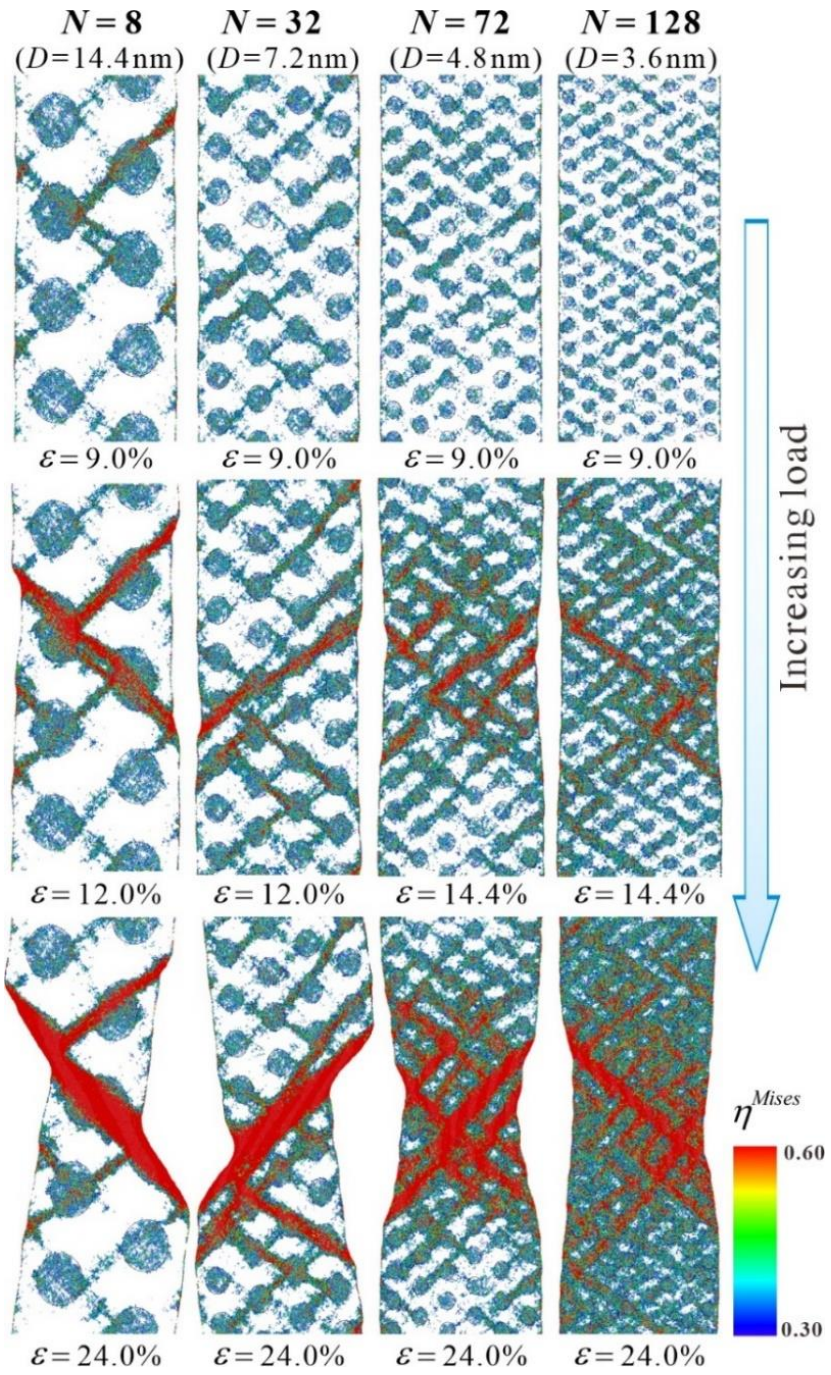

Fig. 10 The deformation patterns for the AB-stacked HMGs with the same volume fraction (26.1%) but different numbers of heterogeneous phases (*D*=14.4 nm, 7.2 nm, 4.8 nm and 3.6 nm from 1st to 4th columns, respectively), demonstrating the transition of the deformation mode.

4. Conclusions

In summary, large-scale MD simulations were carried out to investigate the tensile mechanical properties of Cu64Zr36 (at.%) MGs under various distributed irradiation-rejuvenated phases. Meaningful insights were gained into understanding the effect of pattern distribution, volume fraction and size effect on the deformation behavior of HMGs under tensile loading at ambient temperature. The main conclusions are summarized below:

1) The arrangements of the rejuvenated phases barely affect the elastic behavior but have a nonnegligible effect on the plastic behavior of HMGs. Compared to the AA-stacked arrangement, the AB-stacked one with low diagonal orientation is more effective at promoting strain delocalization, owing to a larger angle deviation from the principal shear stress and a thicker critical SB that reduces the elastic energy release for unstable shear localization.

2) With the increasing volume fraction of the rejuvenated phases from 0% to 58.6%, the deformation behavior of HMGs changes from the highly localized shear banding to the homogeneous-like plastic flow. This is because, when the volume fraction increases to 33.0%, the rejuvenated phases are sufficient large to serve as effective barriers to suppress SB propagation across the rejuvenated phases, which promotes the activation of new SBs and the formation of a network of multiple SBs without one going critical. The formation and interaction of multiple SBs can considerably stabilize the plastic deformation process.

3) The tensile ductility of HMGs can be improved by decreasing the phase size of the rejuvenated phases without sacrifice of the strength. With the finer phase size, the rejuvenated phases are distributed more homogenously in HMGs, which results in the formation of more embryonic SBs at the same applied strain and redistributes more plasticity throughout the sample.

Data availability

The simulation data from this study are available from Prof. K. C. Chan from The Hong Kong Polytechnic University upon reasonable request.

Acknowledgements

The work described in this paper was supported by the Postdoc Matching Fund Scheme of The Hong Kong Polytechnic University (Project No. P0035796/1-W17D), and National Natural Science Foundation of China (Project No. 52201181, 51971097), and a grant from the NSFC/RGC Joint Research Scheme sponsored by the National Natural Science Foundation of China and the Research Grants Council of Hong Kong (Project No. 52061160483 and No. N_PolyU523/20), and National Postdoctoral Science Foundation of China (Project No. 2020M672336).

References

[1] M.X. Li, Y.T. Sun, C. Wang, L.W. Hu, S. Sohn, J. Schroers, W.H. Wang, Y.H. Liu, Nat. Mater., 21 (2022) 165-172.
[2] Y. Chen, C. Tang, J.-Z. Jiang, Prog. Mater. Sci., 121 (2021) 100799.
[3] D. Ouyang, P. Zhang, C. Zhang, L. Liu, Appl. Mater. Today, 23 (2021) 100988.
[4] B.A. Sun, W.H. Wang, Prog. Mater. Sci., 74 (2015) 211-307.
[5] H.F. Zhou, C. Zhong, Q.P. Cao, S.X. Qu, X.D. Wang, W. Yang, J.Z. Jiang, Acta Mater., 68 (2014) 32-41.
[6] E. Ma, J. Ding, Mater. Today, 19 (2016) 568-579.
[7] L. Zhang, R.L. Narayan, B.A. Sun, T.Y. Yan, U. Ramamurty, J. Eckert, H.F. Zhang, Phys. Rev. Lett., 125 (2020) 055501.
[8] Z. Long, P. Tao, G. Wang, K. Zhu, Y. Chen, W. Zhang, Z. Zhao, Y. Yang, Z. Huang, J. Alloys Compd., 912 (2022).
[9] D. Rajpoot, R.L. Narayan, L. Zhang, P. Kumar, H. Zhang, P. Tandaiya, U. Ramamurty, Acta Mater., 213 (2021).
[10] Y. Tang, H.B. Xiao, X.D. Wang, Q.P. Cao, D.X. Zhang, J.Z. Jiang, J. Mater. Sci. Technol, 78 (2021) 144-154.
[11] Q. Yang, C.-Q. Pei, H.-B. Yu, T. Feng, Nano Lett., 21 (2021) 6051-6056.
[12] Y. Li, Y. Wei, K. Zhang, Y. Zhang, Y. Wang, W. Tang, B. Wei, J. Non-Cryst. Solids, 513 (2019) 76-83.
[13] Y. Zhang, W.H. Wang, A.L. Greer, Nat. Mater., 5 (2006) 857-860.
[14] S.-B. Qiu, K.-F. Yao, Appl. Surf. Sci., 255 (2008) 3454-3458.
[15] W. Zhai, L.H. Nie, X.D. Hui, Y. Xiao, T. Wang, B. Wei, J. Mater. Sci. Technol, 45 (2020) 157-161.
[16] J. Pan, Y.P. Ivanov, W.H. Zhou, Y. Li, A.L. Greer, Nature, 578 (2020) 559-562.
[17] S.V. Ketov, Y.H. Sun, S. Nachum, Z. Lu, A. Checchi, A.R. Beraldin, H.Y. Bai, W.H. Wang, D.V. Louzguine-Luzgin, M.A. Carpenter, A.L. Greer, Nature, 524 (2015) 200-203.
[18] J. Saida, R. Yamada, M. Wakeda, Appl. Phys. Lett., 103 (2013).
[19] F. Meng, K. Tsuchiya, Seiichiro, Y. Yokoyama, Appl. Phys. Lett., 101 (2012).

[20] Y.H. Qiu, C. Xu, E.G. Fu, P.P. Wang, J.L. Du, Z.Y. Hu, X.Q. Yan, X.Z. Cao, Y.G. Wang, L. Shao, Intermetallics, 101 (2018) 173-178.
[21] R. Liontas, X.W. Gu, E. Fu, Y. Wang, N. Li, N. Mara, J.R. Greer, Nano Lett., 14 (2014) 5176-5183.
[22] J.C. Qiao, Q. Wang, J.M. Pelletier, H. Kato, R. Casalini, D. Crespo, E. Pineda, Y. Yao, Y. Yang, Prog. Mater. Sci., 104 (2019) 250-329.
[23] L. Zhao, K.C. Chan, S.H. Chen, S.D. Feng, D.X. Han, G. Wang, Acta Mater., 169 (2019) 122-134.
[24] R.E. Baumer, M.J. Demkowicz, Acta Mater., 83 (2015) 419-430.
[25] X.X. Li, J.G. Wang, H.B. Ke, C. Yang, W.H. Wang, Materials Today Physics, 27 (2022).
[26] R. Raghavan, B. Kombaiah, M. Döbeli, R. Erni, U. Ramamurty, J. Michler, Mater. Sci. Eng. A, 532 (2012) 407-413.
[27] D.J. Magagnosc, R. Ehrbar, G. Kumar, M.R. He, J. Schroers, D.S. Gianola, Sci. Rep., 3 (2013) 1-6.
[28] D.J. Magagnosc, G. Kumar, J. Schroers, P. Felfer, J.M. Cairney, D.S. Gianola, Acta Mater., 74 (2014) 165-182.
[29] X.L. Bian, G. Wang, H.C. Chen, L. Yan, J.G. Wang, Q. Wang, P.F. Hu, J.L. Ren, K.C. Chan, N. Zheng, A. Teresiak, Y.L. Gao, Q.J. Zhai, J. Eckert, J. Beadsworth, K.A. Dahmen, P.K. Liaw, Acta Mater., 106 (2016) 66-77.
[30] H. Chen, Y. Hai, G. Wang, X. Liu, J. Xu, W. Yin, J. Alloys Compd., 840 (2020).
[31] L. Zhao, D. Ouyang, Y. Wang, K. Chan, J. Non-Cryst. Solids, 586 (2022) 121559.
[32] S. Plimpton, J. Comput. Phys., 117 (1995) 1-19.
[33] Y.Q. Cheng, E. Ma, H.W. Sheng, Phys. Rev. Lett., 102 (2009) 245501.
[34] Y.S. Yun, B.J. Kim, J.H. Na, H.S. Nam, P.R. Cha, W.T. Kim, D.H. Kim, Intermetallics, 92 (2018) 25-35.
[35] S. Feng, L. Qi, L. Wang, S. Pan, M. Ma, X. Zhang, G. Li, R. Liu, Acta Mater., 95 (2015) 236-243.
[36] W.G. Hoover, Physical review. A, General physics, 31 (1985) 1695-1697.
[37] F. Shimizu, S. Ogata, J. Li, Mater. Trans., 48 (2007) 2923-2927.
[38] A. Stukowski, Modell. Simul. Mater. Sci. Eng., 18 (2010) 015012.
[39] W. Wang, Prog. Mater. Sci., 57 (2012) 487-656.
[40] Y.Q. Cheng, A.J. Cao, E. Ma, Acta Mater., 57 (2009) 3253-3267.
[41] D.Şopu, M.Stoica, J. Eckert, Appl. Phys. Lett., 106 (2015) 211902.
[42] F. Zhang, M.I. Mendelev, Y. Zhang, C.-Z. Wang, M.J. Kramer, K.-M. Ho, Appl. Phys. Lett., 104 (2014) 061905.
[43] Y. Sun, Y. Zhang, F. Zhang, Z. Ye, Z. Ding, C.-Z. Wang, K.-M. Ho, J. Appl. Phys., 120 (2016) 015901.
[44] A. Foroughi, R. Tavakoli, H. Aashuri, J. Non-Cryst. Solids, 481 (2018) 132-137.
[45] A.J. Cao, Y.Q. Cheng, E. Ma, Acta Mater., 57 (2009) 5146-5155.
[46] Y.T. Shen, T.H. Kim, A.K. Gangopadhyay, K.F. Kelton, Phys. Rev. Lett., 102 (2009) 057801.
[47] Z. Fan, J. Ding, E. Ma, Mater. Res. Lett., 6 (2018) 570-583.
[48] Q.-K. Li, M. Li, Mater. Trans., 48 (2007) 1816-1821.

[49] B. Wang, L. Luo, E. Guo, Y. Su, M. Wang, R.O. Ritchie, F. Dong, L. Wang, J. Guo, H. Fu, NPJ Comput. Mater., 4 (2018) 1-11.
[50] D. Şopu, F. Moitzi, N. Mousseau, J. Eckert, Appl. Mater. Today, 21 (2020) 100828.
[51] H. Wagner, D. Bedorf, S. Kuchemann, M. Schwabe, B. Zhang, W. Arnold, K. Samwer, Nat. Mater., 10 (2011) 439-442.
[52] Y.H. Liu, D. Wang, K. Nakajima, W. Zhang, A. Hirata, T. Nishi, A. Inoue, M.W. Chen, Phys. Rev. Lett., 106 (2011) 125504.
[53] F. Zhu, H.K. Nguyen, S.X. Song, D.P. Aji, A. Hirata, H. Wang, K. Nakajima, M.W. Chen, Nat. Comm., 7 (2016) 11516.
[54] Z.-D. Sha, P.S. Branicio, H.P. Lee, T.E. Tay, Int. J. Plast., 90 (2017) 231-241.
[55] C.X. Peng, D. Şopu, Y. Cheng, K.K. Song, S.H. Wang, J. Eckert, L. Wang, Mater. Des., 168 (2019) 107662.
[56] K. Albe, Y. Ritter, D. Şopu, Mech. Mater., 67 (2013) 94-103.
[57] S. Yuan, P.S. Branicio, Int. J. Plast., 134 (2020) 102845.
[58] L. Zhao, K. Chan, S. Feng, X. Lu, S. Chen, G. Wang, J. Alloys Compd., 803 (2019) 193-204.
[59] D. Şopu, S. Scudino, X.L. Bian, C. Gammer, J. Eckert, Scripta Mater., 178 (2020) 57-61.
[60] L. Zhao, D. Han, S. Guan, X. Lu, K. Chan, G. Wang, Mater. Des., 197 (2021) 109246.
[61] D. Şopu, C. Soyarslan, B. Sarac, S. Bargmann, M. Stoica, J. Eckert, Acta Mater., 106 (2016) 199-207.
[62] P. Sun, C. Peng, Y. Cheng, G. Zhang, P. Wang, L. Jia, L. Wang, Comp. Mater. Sci., 163 (2019) 290-300.
[63] S. Yuan, X. Song, P.S. Branicio, Scripta Mater., 186 (2020) 69-73.
[64] S. Yuan, P.S. Branicio, Scripta Mater., 194 (2021) 113639.
[65] B. Sarac, J. Schroers, Nat. Comm., 4 (2013) 1-7.
[66] C.A. Volkert, A. Donohue, F. Spaepen, J. Appl. Phys., 103 (2008) 083539.
[67] J. Eckert, J. Das, S. Pauly, C. Duhamel, J. Mater. Res., 22 (2011) 285-301.
[68] F.-F. Wu, K.C. Chan, S.-T. Li, G. Wang, J. Mater. Sci., 49 (2013) 2164-2170.
[69] S.D. Feng, L. Li, K.C. Chan, L. Qi, L. Zhao, L.M. Wang, R.P. Liu, J. Alloys Compd., 770 (2019) 896-905.